

Received December 26, 2018, accepted January 21, 2019, date of publication January 30, 2019, date of current version April 1, 2019.

Digital Object Identifier 10.1109/ACCESS.2019.2896280

# Modeling and Analysis on Radio Interference of OFDM Waveforms for Coexistence Study

JAEDON PARK<sup>1</sup>, EUNHYOUNG LEE<sup>1</sup>, SUNG-HO PARK<sup>2</sup>, (Member, IEEE),  
SABOGU-SUMAH RAYMOND<sup>3,4</sup>, (Member, IEEE),  
SEONGMIN PYO<sup>5</sup>, (Senior Member, IEEE),  
AND HAN-SHIN JO<sup>4</sup>, (Member, IEEE)

<sup>1</sup>Agency for Defense Development, Daejeon 34186, South Korea

<sup>2</sup>Data Solution, Inc., Seoul 06101, South Korea

<sup>3</sup>National Communications Authority, Accra, Ghana

<sup>4</sup>Department of Electronics and Control Engineering, Hanbat National University, Daejeon 34158, South Korea

<sup>5</sup>Department of Information and Communication Engineering, Hanbat National University, Daejeon 34158, South Korea

Corresponding author: Han-Shin Jo (hsjo@hanbat.ac.kr)

This work was supported in part by the Agency for Defense Development, and in part by the Basic Science Research Program through the National Research Foundation of Korea funded by the Ministry of Science, ICT and Future Planning under Grant NRF-2016R1C1B2011921.

**ABSTRACT** The fifth-generation (5G) cellular mobile communications look promising with features that can help improving consumer experience and satisfaction. To be able to provide these features, more spectrum is required according to the Shannon–Hartley theorem. Spectrum is, however, a finite and scarce resource, and it can be allocated to a new service only when the spectral coexistence with other incumbents is ensured. New waveforms for 5G that differ from the conventional orthogonal frequency-division multiplexing (OFDM) are required in order to have a superior performance in terms of out-of-band emissions and to be able to utilize the fragmented spectrum in different bands. We developed the analytical models for evaluating the out-of-band emissions of the conventional cyclic prefix (CP)-OFDM as well as its alternatives: windowed OFDM and filtered OFDM, using their signal spectral modeling. The resulting expressions for the power spectral density (PSD) and the frequency-dependent rejection (FDR) involve simple closed-form expressions or easily computable integrals. We applied the expressions to the advanced minimum coupling loss model for assessing the feasibility of the spectral coexistence between the potential 5G systems (with linearized or nonlinear power amplifier) and the incumbent radar systems. The numerical simulation results indicate that both the windowed OFDM and filtered OFDM guarantee the coexistence at the low expense of the spectrum utilization and their coexistence performance can be reduced and reversed with nonlinearity distortion of the power amplifier.

**INDEX TERMS** Coexistence study, CP-OFDM, fifth-generation (5G) cellular mobile communications, filtered OFDM, frequency dependent rejection, frequency sharing study, out-of-band emission, power amplifier nonlinearity, power spectral density.

## I. INTRODUCTION

### A. BACKGROUND AND MOTIVATION

Orthogonal Frequency Division Multiplexing (OFDM) has been used successfully for fourth-generation (4G) and other wireless communication systems. Despite the success of OFDM-based waveforms, it has its sets of disadvantages such as high peak-to-average power ratio (PAPR), the large tail of

a sinc shaped spectrum leading to high out-of-band emission, etc. Notwithstanding the fact that OFDM presents high spectrum efficiency through orthogonal frequency multiplexing, its out-of-band emission may not be acceptable without guard bands [1]. In 4G LTE specifically, about 10% of the allocated bandwidth is reserved as a guard band to allow room for the signals to attenuate in order to meet the spectrum mask. However, this is a complete waste of the precious spectrum resource. The frequency and the time resources in OFDM are uniformly divided into several equal-sized elements to

The associate editor coordinating the review of this manuscript and approving it for publication was Shihao Yan.

carry information. In order to achieve orthogonality and to avoid either inter-symbol or channel interference, strict time and frequency alignment are needed. This results in heavy signaling to achieve the perfect synchronization, especially for the uplink transmission. An imperfect synchronization can lead to suboptimal performance.

Futuristic fifth-generation (5G) systems promise several advantages over previous systems, including high data rates, ultra-reliable low latency communication (URLLC), high spectral efficiency, massive connectivity, and improved energy efficiency [2]. In order to reap the benefits of 5G, new and efficient waveforms have been proposed by the industry experts and academia. So far, we know of the following proposed waveforms for 5G; windowed OFDM [3], [4], filter-bank multicarrier (FBMC) [5]–[7], universal filtered multicarrier (UFMC) [8], filtered OFDM [1], [9]–[12], and fast convolution filtered CP-OFDM (FC-F-OFDM) [13], [14].

Filtering is a proven and effective way of suppressing sidelobes in OFDM. UFMC was introduced by Alcatel-Lucent [8], where filtering is applied to a block of consecutive subcarriers, which provides low out-of-band emission. In multipath channels, UFMC severely suffers from high intersymbol interference leading to suboptimal performance. In filtered OFDM, the available bandwidth is divided into many sub-bands. This enables the support of a different set of services in different sub-bands with appropriately time-domain filtered waveforms [1], [9]. On the other hand, Yli-Kaakinen *et al.* [13] proposed frequency-domain filtering approach with lower computational complexity and increased flexibility compared to the time-domain filtering. The filter design is based on optimized frequency domain windows that allows the balancing of the required minimum stopband attenuation, transition bandwidth, and error vector magnitude (EVM) performance.

Once spectrum sidelobes are reduced, a greater power of the signal is concentrated in the main lobe that helps in reducing the leakage power in the adjacent channel. In [8] block OFDM waveform was proposed that demonstrated an excellent frequency localization and can be integrated with the OFDM techniques and LTE principles. The literature [10] considered the low energy features of filtered OFDM signals in the guard band and proposed a novel resource sharing method to mitigate the cellular-user-induced interference on the D2D receiver. Also in [11], the superiority of the filtered OFDM over the conventional OFDM was shown in terms of sidelobe suppression. Zhang *et al.* [12] established a mathematical model for a filtered OFDM system and a multirate filtered OFDM was also proposed to enable a low-complexity low-cost communication scenario, such as narrow-band internet-of-things (IoT). However, these works do not present anything in favor of coexistence and neither do they present any analytical expression for evaluating the amount of out-of-band emission.

Many countries are planning the use of 3 GHz for initial 5G services, along with millimeter wave frequency

band [15], [16]. However, the 3 GHz band is allocated to the radiolocation services in quite many countries, and a study on spectral coexistence (in-band or adjacent band compatibility) between the two services is essential for worldwide launch of 5G services. The spectral coexistence is typically assessed by calculating the potential radio interference power at an incumbent receiver (operating in-band or adjacent band) emitted from a new radio system and vice versa. On the basis of the interference calculation, the geographic and/or the spectral isolations to satisfy the predefined permissible interference level are quantified in general. Furthermore, the technical and operational measures as described in Table 1 could be proposed for attenuating the interference and accordingly ensuring the coexistence. This study, diversely named as *coexistence study*, *compatibility study*, *sharing study*, *frequency sharing study*, etc. in wireless standard activities, is an essential prerequisite for international or regional spectrum allocation (or coordination) conducted by the International Telecommunication Union-Radiocommunication (ITU-R) as well as each nation’s spectrum management. In fact, World Radiocommunication Conference 2015 (WRC-15) requested ITU-R to perform a further study on coexistence between International Mobile Telecommunication (IMT) in the frequency band 3,300–3,400 MHz and radiolocation service below 3,300 MHz [17]. The ITU-R Report M.2111 [18] informs that significant frequency separation (greater than 59 MHz) is required to protect typical shipborne radars in 3 GHz band. It is crucial to study how much the new OFDM waveforms for 5G can reduce the frequency separation and enhance the efficiency of the spectrum utilization.

TABLE 1. Interference mitigation techniques.

Classification	Techniques
Transmitting power	<ul style="list-style-type: none"> <li>- Specifying reduced power limit of BS</li> <li>- Adjustment of radiating patterns of transmitting antennas to reduce the EIRP in the direction of radar receivers</li> </ul>
Radio equipment deployment	<ul style="list-style-type: none"> <li>- Interference dependent IMT deployment (i.e. BS density, cell radius)</li> </ul>
Spectrum mask	<ul style="list-style-type: none"> <li>- Specific masks of out-band and spurious emissions of base stations, which could be achieved by using specific RF filters in BS transmitters</li> </ul>
Frequency gap	<ul style="list-style-type: none"> <li>- Sufficiently large guard band between IMT and radar systems</li> </ul>
Propagation characteristics	<ul style="list-style-type: none"> <li>- Clutter losses, antenna heights, terrain relief and masking from buildings for specifying the most appropriate network topology of base stations.</li> </ul>

**B. RELATED WORKS AND CONTRIBUTIONS**

Modeling and analyzing the amount of out-of-band emission of the OFDM waveforms is essential for the 5G coexistence study. Modeling the Power Spectral Density (PSD) of an OFDM waveform with zero guard interval (neither windowed nor filtered), Jo *et al.* [19] derived an analytic expression for the fraction of out-of-band OFDM power

within the band of a victim receiver, named as interfering signal power loss. The mathematical expression is then applied to the coexistence study of fixed microwave point-to-point systems with OFDM-based IMT systems. The initial work has been extended to the analytical method, called the Advanced Minimum Coupling Loss (A-MCL) method for modeling the interference of OFDM systems with flexible spectrum usage [20]. The A-MCL method is further polished for the various coexistence studies [21]–[23]. Leveraging the PSD model of transmitting waveforms, the A-MCL method is beneficial in allowing for an accurate theoretical description of the spectral coexistence of wireless standards with flexible spectrum usage as well as static spectrum usage.

In order to address the coexistence problem between the wireless standards, literature developed effective ways to alleviate the problem of spectrum paucity. Spatial, temporal, frequency, and cognitive radio techniques are used to enable the wireless systems coexistence. For example, Raymond *et al.* [24], [25] proposed and implemented the spatial and temporal techniques employed at the LTE system to share with the primary surveillance radar. Most of their modeling was based on the development of power control algorithms with little or no emphasis on the out-of-band emission of the systems considered. Projection of the cellular system's signals onto the null space of a primary radar was studied in [26] using a blinding learning technique developed in [27].

The coexistence of 5G with other services is studied in the recent literature, Guidolin *et al.* They addressed the coexistence of fixed satellite service (FSS) and cellular networks, where the inference from the cellular BS to the FSS earth station in the 18 GHz band [28] and the interference from the cellular BS to the FSS earth station in the 28 GHz band [29] are evaluated. Kim *et al.* [30] considered the coexistence of 5G with incumbents in 28 GHz and 70 GHz millimeter wave spectrum. An extensive co-channel sharing scenario was considered to determine the minimum spatial separation from the primary user. Hattb *et al.* [31] analyzed the impact of 5G coexistence on the fixed stations using actual building databases. Hassan *et al.* [32] introduced the current status for spectrum usage in the Malaysian 5G candidate bands and evaluated the feasibility of coexistence between 5G and incumbent fixed services in the 28 GHz band. Using the Monte Carlo (MC) simulation, Kim *et al.* [33] computed the amount of interference rejection that is required to protect a fixed service system from 5G small cell networks at millimeter wave frequency bands, where at least 8.6 km, 5.5 km, and 1 km separation are respectively required for 28 GHz, 38 GHz, and 60 GHz 5G systems. In [34], the first results on coexistence between 5G NR and LTE uplink are presented. Although all of these aforementioned works provided valuable information and technologies, none of them conducted a comparative study of 5G waveform candidates as well as conventional CP-OFDM for its coexistence with an analytical framework.

This work differs from other works in the following ways: First, we derived the closed-form (or quasi-closed) expressions for the PSD of cyclic prefix (CP)-OFDM, windowed OFDM, and filtered OFDM, from which the analytical expressions for the Frequency Dependent Rejection (FDR) of the OFDM waveforms are derived to quantify the number of their out-of-band emissions. Although not given in closed-form, the FDR expressions are easily implemented by numerical computing software, such as MATLAB. Moreover, we leveraged the FDR expressions to develop a new A-MCL model for evaluating the feasibility of the coexistence between incumbent radar systems and future 5G systems using the CP-OFDM, windowed OFDM and filtered OFDM. We also adopted the statistical clutter loss model newly developed by ITU for more accurate interference assessment. To the best of the authors' knowledge, this work is the first to develop an analytical model for evaluating the potential coexistence of 5G with other incumbent systems using the proposed waveforms.

We modeled the radio frequency interference for generic coexistence study in Section II, and derived the FDRs for the three types of OFDM waveforms in Section III. Section IV presents background and technical models for coexistence study on the radar interfered with 5G in the 3 GHz band. Sections V contains the numerical results that show the effect of the OFDM waveforms on the 5G coexistence with the radar. Concluding remarks and further applications are finally proposed in Section VI.

## II. RADIO INTERFERENCE MODELING FOR COEXISTENCE STUDY

In modeling radio frequency interference for coexistence study, three basic methods can be applied. The first method is the minimum coupling loss (MCL) method which is very simple and static as well as deterministic in nature as it analyses a single interferer and a single victim [35]. It takes relatively very short time to implement. Despite the merits of this method, it produces very pessimistic results which cannot be entirely relied on for establishing the feasibility of coexistence. Secondly, the Monte Carlo (MC) method is accurate and very reliable as it analyses multiple interferers and victims. It models the system in a stochastic fashion to compute the aggregate interference [35], [36]. Its implementation is time consuming. The enhanced MCL (E-MCL) method is an intermediate between the MCL and the MC [35]. The results produced by the E-MCL method are more accurate than the MCL but less reliable as compared to the MC method. The A-MCL method [20] is an extension of MCL with PSD analysis, which is a basic framework for this study.

Radio frequency interference, which is the signal emitted from an undesired transmitter, could degrade performances of a victim receiver. The power level of interference at the victim receiver's input (IF output) is generally given as [37]–[39]

$$I = P_T - L_{FL,T} + G_T + G_R - L_{FL,R} - L_{POL} - L_P - L_{FDR}, \quad (1)$$

where  $P_T$  is output power of the transmitter in dBW,  $L_{FL,T}$  is feeder link losses between output of the transmitter and input of the transmitting antenna,  $G_T$  and  $G_R$  are gains of the transmitting and the receiving antennas,  $L_{FL,R}$  is feeder link losses between output of the receiving antenna and the receiver input,  $L_{POL}$  is loss due to polarization mismatch of the receiving antenna,  $L_P$  is propagation loss (incorporating clutter loss) between transmitting and receiving antennas, and  $L_{FDR}$  is loss due to FDR.

The FDR is a measure of the rejection produced by the receiver selectivity curve on an unwanted transmitter emission spectra. FDR is given by

$$L_{FDR} = 10 \log_{10} \left( \frac{\int_{-\infty}^{\infty} \Phi(f) df}{\int_{-\infty}^{\infty} \Phi(f) \Psi(f - \Delta f) df} \right), \quad (2)$$

where  $\Phi(f)$  is the PSD of the complex baseband equivalent representation (or complex envelop) of the real-valued radio interfering signal,  $\Psi(f)$  is the normalized frequency response of the receiver, and  $\Delta f$  is the frequency offset between the interfering transmitter and the victim receiver as shown in Fig. 1. For the ideal flat response of  $\Psi(f - \Delta f)$  for  $\Delta f - W_v/2 \leq f \leq \Delta f + W_v/2$ , FDR is simplified as

$$L_{FDR} = 10 \log_{10} \left( \frac{\int_{-\infty}^{\infty} \Phi(f) df}{\int_{\Delta f - W_v/2}^{\Delta f + W_v/2} \Phi(f) df} \right), \quad (3)$$

where  $W_v$  is the channel bandwidth of a victim receiver. The area of a signal PSD is equal to the signal power, and thus we obtain the equation of  $P_T = 10 \log_{10} (\int_{-\infty}^{\infty} \Phi(f) df)$ .

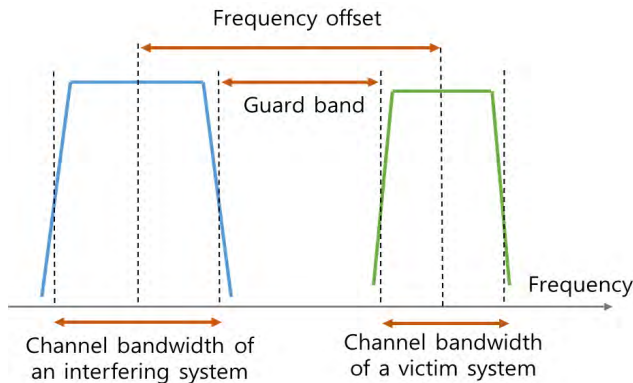


FIGURE 1. Frequency offset and guard band between an interfering transmitter and a victim receiver.

The coexistence is ensured when the interference power given in (1) is less than the interference threshold which is given by

$$I_{th} = INR_{th} + N_R, \quad (4)$$

where  $INR_{th}$  is the interference-to-noise ratio in dB at the receiver input necessary to maintain acceptable performance, and  $N_R$  is the receiver inherent noise level in dBm given by

$$N_R = 10 \log_{10}(k_B T B) + NF, \quad (5)$$

where  $k_B$  is the Boltzmann constant,  $T$  is the absolute temperature,  $B$  is the receiver IF bandwidth,  $NF$  is the receiver noise figure in dB.

Basically, the results of coexistence study are given in terms of the *protection distance* and the *frequency separation*. The protection distance is the minimum geographical separation between the interfering and victim systems that satisfies the condition of  $I \leq I_{th}$ , depending on the propagation loss of the interfering-to-victim link. The frequency separation is generally measured in terms of the frequency offset or the guard band illustrated in Fig. 1, mainly depending on the FDR.

### III. FREQUENCY-DEPENDENT REJECTION OF OFDM WAVEFORMS

As shown in (3), FDR is mainly dependent on the PSD of the transmitting signal. We derived the analytic expression of the PSD of OFDM waveforms, from which their FDRs is obtained. Some promising popular OFDM waveforms for the current or future wireless standards, i.e. CP-OFDM, windowed OFDM, and the filtered OFDM with time-domain filtering are discussed. Another promising frequency-domain filtering based FC-F-OFDM is not studied, since its frequency-domain window weights are not given in the deterministic but is given by nonlinear optimization which precludes deriving analytic expression.

#### A. CP-OFDM

The transmitted baseband signal of CP-OFDM, i.e. the complex envelope of the real-valued transmitted CP-OFDM signal can be expressed as

$$s(t) = \sum_{n=-\infty}^{\infty} \sum_{k=0}^{N-1} c_{n,k} p(t - n(T_s + T_g)) e^{-j2\pi k \frac{1}{N}(T_s + T_g)}, \quad (6)$$

where  $c_{n,k}$  denotes the complex-valued data symbol modulated on the  $k$ th subcarrier of the  $n$ th OFDM symbol,  $p(t)$  is the pulse shaping window,  $T_{tot} = T_s + T_g$  is the total symbol duration,  $T_s$  and  $T_g$  is the data symbol duration and the guard interval, respectively.

Under the assumption that the complex signals at each subcarrier are statistically independent and mutually orthogonal, the PSD expression of the OFDM signal with arbitrary pulse shaping is given as [3], [4]

$$\Phi_s(f) = \frac{P_s}{T_{tot}} \sum_{k=0}^{N-1} \left| P\left(f - \frac{k}{T_s}\right) \right|^2, \quad (7)$$

where  $P_s$  represents the variance of the data symbols  $c_{n,k}$  as well as the power of a single OFDM subcarrier,  $1/T_s$  is the subcarrier spacing, and  $P(f)$  is the Fourier transform of the pulse shaping window. We apply a rectangular pulse shaping to (6), defined as

$$p(t) = \Pi\left(\frac{t - T_{tot}/2}{T_{tot}}\right),$$

$$\text{where } \Pi\left(\frac{t}{T_{\text{tot}}}\right) = \begin{cases} 0 & \text{if } |t| > \frac{T_{\text{tot}}}{2} \\ \frac{1}{2} & \text{if } |t| = \frac{T_{\text{tot}}}{2} \\ 1 & \text{if } |t| < \frac{T_{\text{tot}}}{2}. \end{cases} \quad (8)$$

Using the time shifting property of the Fourier transform,  $|P(f)|^2$  is expressed as

$$\begin{aligned} |P(f)|^2 &= |\mathfrak{F}\{p(t)\}|^2 \\ &= \left| \mathfrak{F}\{\Pi(t/T_{\text{tot}})\} e^{-j\pi T_{\text{tot}} f} \right|^2 \\ &= |\mathfrak{F}\{\Pi(t/T_{\text{tot}})\}|^2 \\ &= T_{\text{tot}}^2 \text{sinc}^2(T_{\text{tot}} f), \end{aligned} \quad (9)$$

where the sinc function is defined as  $\text{sinc}(x) = \sin(\pi x)/\pi x$  for  $x \neq 0$ , otherwise it is equal to one.

Combining (7) and (9), the PSD of CP-OFDM with rectangular pulse shaping is given by

$$\Phi_s^{(\text{CP})}(f) = P_s T_{\text{tot}} \sum_{k=0}^{N-1} \left\{ \text{sinc}\left[\left(f - \frac{k}{T_s}\right) T_{\text{tot}}\right] \right\}^2, \quad (10)$$

From (3) and (10), we obtain a closed-form expression for the FDR of CP-OFDM, given by

$$\begin{aligned} L_{\text{FDR}}^{(\text{CP})} &= P_T - 10 \log_{10} \left( \frac{P_s}{\pi} \sum_{k=0}^{N-1} \left[ \frac{\sin^2(f_k^-)}{f_k^-} - \frac{\sin^2(f_k^+)}{f_k^+} \right. \right. \\ &\quad \left. \left. - \text{Si}(2f_k^-) + \text{Si}(2f_k^+) \right) \right], \end{aligned} \quad (11)$$

where  $\text{Si}(x) = \int_0^x \sin t/t dt$  is the sine integral, and  $f_k^+ = \pi T_{\text{tot}} (\Delta f + W_v/2 - k/T_s)$  and  $f_k^- = \pi T_{\text{tot}} (\Delta f - W_v/2 - k/T_s)$ . Equation (11) is derived in Appendix A. It should be noted that (11) is the expanded result of our previous study in [20]. In other words, for zero guard interval, (10) is the same as [20, eq. (2)]. Moreover, we can compute FDR way more easily using (11) without the infinite summation presented in (5) of [20].

### B. WINDOWED OFDM

To suppress out-of-band emissions, windowed OFDM adopts smooth time-windowing functions for pulse shaping. As a typical example, a raised cosine function,  $w_{\text{rc}}(t)$ , of duration  $T_w = T_{\text{tot}} + T_{\text{tr}}$  is adopted, given by

$$\begin{aligned} p(t) &= w_{\text{rc}}\left(t - \frac{T_{\text{tot}}}{2}\right), \quad \text{where} \\ w_{\text{rc}}(t) &= \begin{cases} 1 & 0 \leq |t| < (T_{\text{tot}} - T_{\text{tr}})/2 \\ \frac{1}{2} \left( 1 + \cos\left(\frac{\pi(|t| - (T_{\text{tot}} - T_{\text{tr}})/2)}{T_{\text{tr}}}\right) \right) & (T_{\text{tot}} - T_{\text{tr}})/2 \leq |t| < (T_{\text{tot}} + T_{\text{tr}})/2 \\ 0 & (T_{\text{tot}} + T_{\text{tr}})/2 \leq |t|, \end{cases} \end{aligned} \quad (12)$$

where  $T_{\text{tr}}$  is the transition time.

From (7) and the Fourier transform of (12), the PSD of the windowed OFDM is given by

$$\begin{aligned} \Phi_s^{(\text{W})}(f) &= P_s T_{\text{tot}} \sum_{k=0}^{N-1} \left\{ \text{sinc}\left[\left(f - \frac{k}{T_s}\right) T_{\text{tot}}\right] \right. \\ &\quad \left. \times \frac{\cos\left(\pi T_{\text{tr}}\left(f - \frac{k}{T_s}\right)\right)}{1 - 4T_{\text{tr}}^2\left(f - \frac{k}{T_s}\right)^2} \right\}^2. \end{aligned} \quad (13)$$

It should be noted that (13) is found in [3] and [4], in which, the deriving process of  $W_{\text{rc}}(f)$  is not given in detail. We have thus provided a whole deriving process in Appendix B, which is highly applicable for the diverse forms of the raised cosine function. From (3) and (13), FDR of the windowed OFDM is given by

$$\begin{aligned} L_{\text{FDR}}^{(\text{W})} &= P_T - 10 \log_{10} \\ &\quad \times \left[ P_s T_{\text{tot}} \sum_{k=0}^{N-1} \int_{\Delta f - W_v/2}^{\Delta f + W_v/2} \left\{ \text{sinc}\left[\left(f - \frac{k}{T_s}\right) T_{\text{tot}}\right] \right. \right. \\ &\quad \left. \left. \times \frac{\cos^2\left(\pi T_{\text{tr}}\left(f - \frac{k}{T_s}\right)\right)}{\left(1 - 4T_{\text{tr}}^2\left(f - \frac{k}{T_s}\right)^2\right)^2} \right\} df \right]. \end{aligned} \quad (14)$$

Although not closed-form expression, (14) can be easily implemented by numerical computing software. The FDR of the windowed OFDM is only affected by the three parameters;  $T_{\text{tr}}$ ,  $T_s$ , and  $T_{\text{tot}}$ , which is useful for OFDM system design controlling co-channel and adjacent channel interference.

### C. FILTERED OFDM

The filtered OFDM signal  $x(t)$  is obtained by passing the CP-OFDM signal  $s(t)$  in (6) through a spectrum shaping filter. Thus,  $x(t)$  is given by the convolution of  $s(t)$  and the filter's impulse response  $h(t)$  as follows:

$$x(t) = s(t) * h(t). \quad (15)$$

We adopted the spectrum shaping filter presented in [9], which is designed from the soft truncation of a basic filter. The soft truncation is conducted by applying a time-window function,  $w(t)$  to the impulse response of the basic filter,  $g(t)$ . The impulse response of the softly truncated filter is given by

$$h(t) = g(t) \cdot w(t). \quad (16)$$

Here, we considered the sinc function of  $g(t) = W_g \text{sinc}(W_g t)$ , whose frequency response is the rectangular window with bandwidth  $W_g$ , i.e.  $\Pi(f/W_g)$ . To suppress out-of-band emissions, the basic filter is softly truncated by adopting smooth time-windowing functions such as Hanning, Hamming, and Blackman windows. As a typical example, the Hanning window of duration  $T_w$  is adopted, given by

$$w(t) = \begin{cases} \frac{1}{2} + \frac{1}{2} \cos\left(\frac{2\pi|t|}{T_w}\right) & |t| \leq \frac{T_w}{2} \\ 0 & |t| > \frac{T_w}{2}, \end{cases} \quad (17)$$

The PSD of the filtered OFDM signal is given by

$$\Phi_x(f) = \frac{P_s T_{\text{tot}}}{16\pi^2} [2\text{Si}(\pi f_u) - 2\text{Si}(\pi f_l) + \text{Si}(\pi - \pi f_l) - \text{Si}(\pi - \pi f_u) + \text{Si}(\pi + \pi f_u) - \text{Si}(\pi + \pi f_l)]^2 \times \sum_{k=0}^{N-1} \left\{ \text{sinc} \left[ \left( f - \frac{k}{T_s} \right) T_{\text{tot}} \right] \right\}^2, \quad (18)$$

where  $f_u = T_w (f + W_g/2)$ , and  $f_l = T_w (f - W_g/2)$ . Equation (18) is derived in Appendix C. It should be noted that PSD of the filtered OFDM can be found in quasi-closed form since  $\text{Si}(x)$  can be evaluated as easily as a basic trigonometric function by a numerical computing software. From (3) and (18), the FDR of the filtered OFDM is given by

$$L_{\text{FDR}}^{(F)} = P_T - 10 \log_{10} \left[ \frac{P_s T_{\text{tot}}}{16\pi^2} \sum_{k=0}^{N-1} \int_{\Delta f - W_v}^{\Delta f + W_v} \text{sinc} \left( \left( f - \frac{k}{T_s} \right) T_{\text{tot}} \right)^2 \times \{2\text{Si}(\pi f_u) - 2\text{Si}(\pi f_l) + \text{Si}(\pi - \pi f_l) - \text{Si}(\pi - \pi f_u) + \text{Si}(\pi + \pi f_u) - \text{Si}(\pi + \pi f_l)\}^2 df \right]. \quad (19)$$

Although not closed-form expression, (19) is analytically tractable and can be easily implemented by a numerical computing software. The FDR of the filtered OFDM is only affected by the four parameters;  $T_w$ ,  $T_s$ ,  $T_{\text{tot}}$ , and  $W_g$ , which is useful for the OFDM system design controlling co-channel and adjacent channel interference.

### D. PERFORMANCE COMPARISON

The simulation parameters are presented in Table 2. A typical value of LTE systems with 10 MHz channel is adopted. The PSDs of CP-OFDM, windowed OFDM, and filtered OFDM are shown in Fig. 2. The simulated PSDs are almost close to the analytical results. Out-of-band emission of the filtered OFDM is remarkably reduced compared to the other two OFDM waveforms.

FDRs versus guard band for the three OFDM waveforms are plotted in Fig. 3. The guard band is defined as the frequency separation between the innermost edges of the channel of interfering LTE BS and the channel of the victim receiver as shown in Fig. 1. Since the lower level of out-of-band emission results in the smaller denominator in (3), FDR increases in the order of CP-OFDM, windowed OFDM, and filtered OFDM. It should be noted that even adopting larger guard band is not effective in ensuring coexistence between the CP-OFDM and other radio systems because of slow increase in the FDR. Whereas, interference power from the filtered OFDM and windowed OFDM are significantly attenuated for smaller guard band. The results in Figs. 2 and 3 are obtained by assuming a linearized power amplifier that could be achieved by joint peak to average power ratio (PAPR) reduction and linearization [40]–[42].

TABLE 2. Simulation parameters and assumptions.

Parameter	Symbol	Units	Value
Channel bandwidth		MHz	10
Signal bandwidth	-	MHz	9
Output power	-	dBm	46
Number of DFT points			1024
Number of data subcarriers	$N$	-	600
Subcarrier spacing	$1/T_s$	kHz	15
Sampling rate		MHz	15.36
Hanning window duration	$T_w$	us	33.33
Number of samples of Hanning window			513
Transition time	$T_{tr}$	us	6.77
Number of samples of transition time			104
Data symbol duration	$T_s$	us	66.66
Number of samples of Data symbol duration			1024
Guard interval	$T_g$	us	4.69
Number of samples of guard interval			72
Channel bandwidth of a victim system	$W_v$	MHz	10

### E. POWER AMPLIFIER NONLINEARITY

Nonlinear distortion due to power amplifier degrades signal quality. Most power amplifiers currently applied to wireless communication devices are solid-state power amplifiers. A mathematical equation was developed for modeling the behavior of solid-state power amplifiers by Christopher Rapp. The Rapp model [43] is one of the most commonly used models for solid-state power amplifiers and its amplitude-to-amplitude (AM-AM) distortion, is given by

$$V_{\text{out}} = \frac{V_{\text{in}}}{\left( 1 + \left( \frac{|V_{\text{in}}|}{V_{\text{sat}}} \right)^{2p} \right)^{\frac{1}{2p}}}, \quad (20)$$

where  $V_{\text{sat}}$  is the input saturation voltage of power amplifier and  $p$  is the smoothness factor. Rapp models for varying  $p$ , as shown in Fig. 4, produce a smooth transition for the envelope characteristic as the input amplitude approaches saturation. In practice, to mitigate the impacts of the nonlinear distortion, the power amplifier operates at an input back-off (IBO) from a given saturation level as follows.

$$IBO = 10 \log_{10} \left( \frac{V_{\text{sat}}^2}{\sigma^2} \right), \quad (21)$$

where  $\sigma^2$  is the mean power of the signal input to the power amplifier.

OFDM modulation with nonconstant envelope signals needs to be 6 to 12 dB back off for the power amplifier to operate in a more linear region [44]. From IEEE standards documentation, it is commonly accepted that the Rapp model

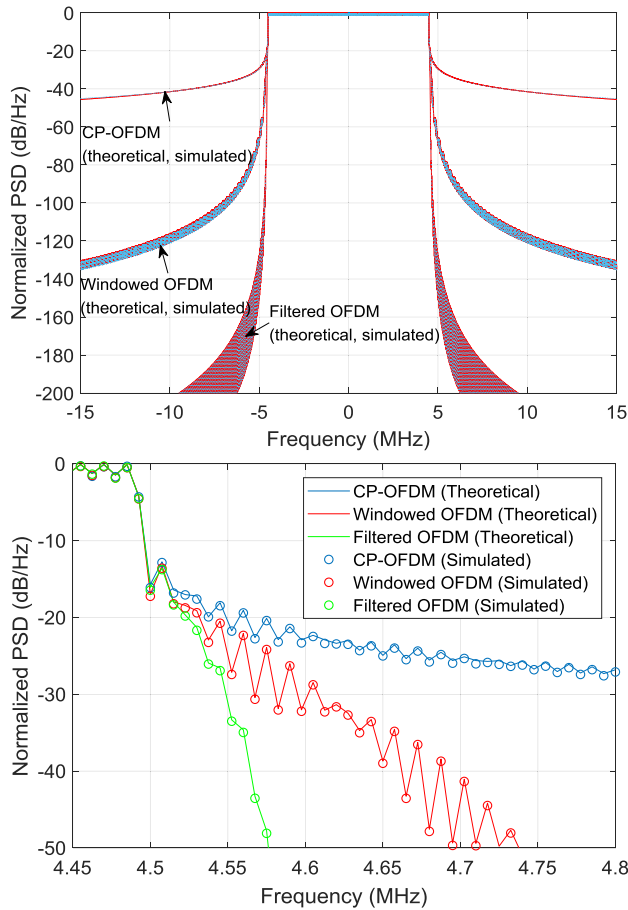


**FIGURE 2.** PSD of CP-OFDM, windowed OFDM, and filtered OFDM: A general view showing both in-band and out-of-band (upper figure), and its zoomed in figure (lower figure).

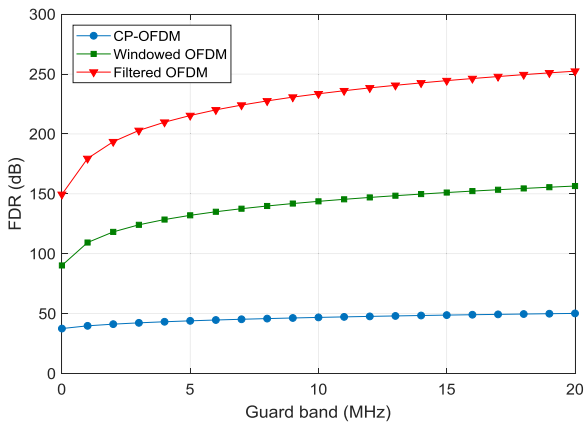


**FIGURE 3.** FDR of CP-OFDM, windowed OFDM, and filtered OFDM for 10 MHz IF bandwidth of victim receiver.

with the values of  $p$  within the range of 2 to 3 well captures the nonlinearity of the realistic power amplifiers [45], but the values of  $p$  around 1 are also used in the literature [46], [47]. We thus, obtain the simulation results of PSD and FDR for IBO of 10 dB and  $p = 1, 2,$  and  $3$ .

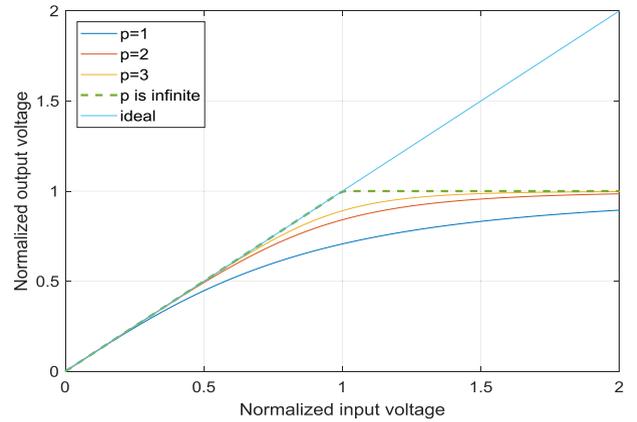


**FIGURE 4.** AM-AM characteristic of Rapp model for varying smoothness factor.

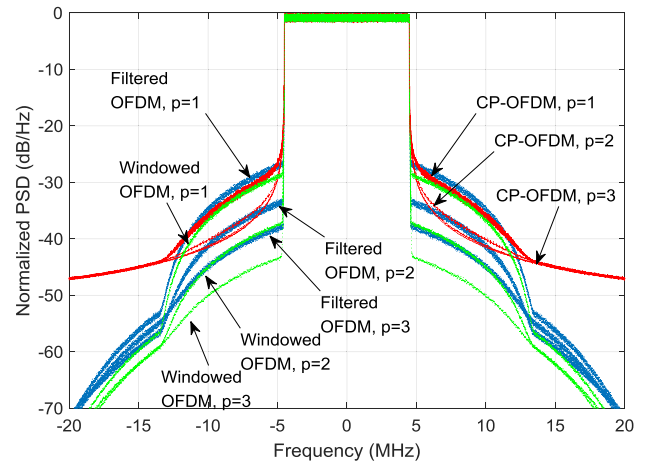


**FIGURE 5.** PSD of CP-OFDM (red curves), windowed OFDM (green curves), and filtered OFDM (blue curves) distorted by power amplifier nonlinearity for various smoothness factors  $p$ , and IBO = 10 dB.

Figs. 5 and 6 show the PSDs and FDRs considering power amplifier nonlinearity, respectively. Unlike in Fig. 3, windowed OFDM PSD has a lower sidelobe as compared to the filtered OFDM for all values of  $p$ . Moreover, filtered OFDM PSD level in the adjacent band of 5 to 12 MHz is the highest for  $p = 1$ , which results in the lowest FDR of filtered OFDM as shown in Fig. 6(a). It should be noted that the sidelobe suppression performance of windowed and filtered OFDM can be reversed depending on the power amplifier nonlinearity.

#### IV. COEXISTENCE BETWEEN 5G IMT AND RADAR IN 3 GHz BAND: TECHNICAL CHARACTERISTICS AND MODELS

##### A. BACKGROUND

There is globally a growing interest in using the frequency bands in 3.3–3.8 GHz for initial commercial 5G services. Some countries have specified the spectrum band for 5G service (e.g., 3.7–4.2 GHz in the US, 3.4–3.8 GHz in EU, and 3.4–3.7 GHz in Korea, and 3.3–3.6 GHz in China) [15], [16].

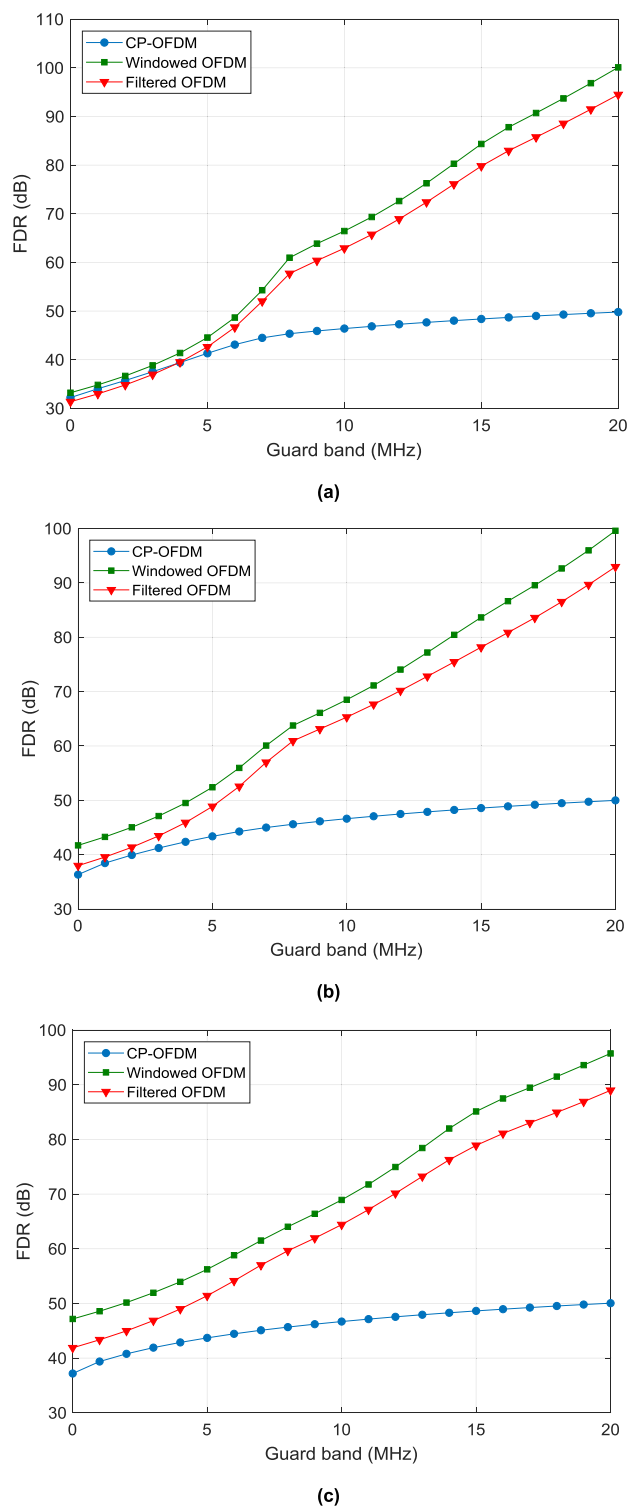


**FIGURE 6.** FDR comparison of OFDM waveforms distorted by power amplifier nonlinearity, IBO = 10 dB. (a)  $p = 1$ , (b)  $p = 2$ , (c)  $p = 3$ .

Meanwhile, in the ITU Radio Regulations (RR) [48], the frequency band 3,100–3,300 MHz is allocated to the radiolocation service on a primary basis, and earth exploration and space research on a secondary basis. The frequency band

3,300–3,400 MHz is also predominantly used for radar systems in a number of countries across the world. Whereas, a significant number of countries have no deployments in the band. At WRC-15, the band was allocated, on a primary basis, to the mobile service in a number of countries in accordance with RR footnotes 5.429, 5.429A, 5.429C and 5.429E. The band was also allocated for IMT, in accordance with RR footnotes 5.429B, 5.429D and 5.429F, in many other countries.

A lot of studies have already been carried out at ITU-R to discuss the potential coexistence of IMT systems with radar systems in the 3 GHz frequency range [18], [49]. Nevertheless, WRC-15 requested ITU-R to perform further work on compatibility and coexistence in this band. This is in Resolution 223 [17], which invites ITU-R, among other things to further study adjacent band compatibility between IMT in the frequency band 3,300–3,400 MHz and radiolocation service below 3,300 MHz. In this context, we compare the results on the coexistence between 5G IMT with CP-OFDM, windowed OFDM, or filtered OFDM in 3,300–3,400 MHz and radar systems below 3,300 MHz.

### B. INTERFERENCE SCENARIO

A coastal area scenario is considered where a 5G IMT BS is assumed to be located at a shoreline in Incheon, Korea as shown in Fig. 7. Ship-based radiolocation radars B and C defined in Recommendation ITU-R M.1465 [50] receive interference from the single entry 5G IMT BS operating in the adjacent channel. The radar channels are centered at 3,300 MHz and the channel of 5G IMT BS is centered at a higher frequency with a given guard band. The worst case is studied where the peak antenna gain is taken for the radars, and peak antenna gain with a loss due to the antenna tilting is applied for the BS as shown in Fig. 7. Owing to much lower EIRP of 5G IMT user equipment (UE), the separation distance required to protect radars from the UE would be much shorter than the distance required to protect from 5G IMT BS. The interference due to 5G IMT UE is consequently not assessed in this paper.

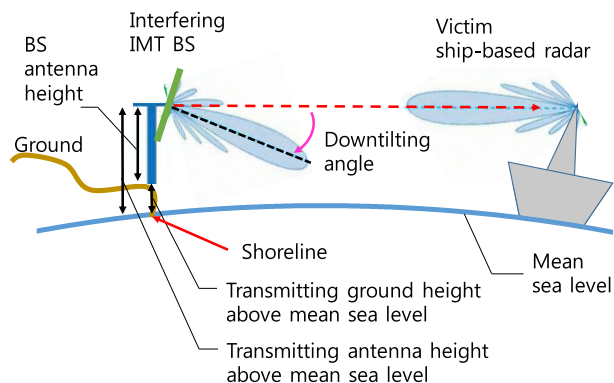


**FIGURE 7.** Illustration of interference scenario and antenna related parameters.

C. TECHNICAL CHARACTERISTICS

Table 3 presents generic BS characteristics configured in the Report ITU-R M.2292 [51]. Recommendation ITU-R M.1465 [50] provides radiolocation radar characteristics operating in the frequency range 3,100–3,700 MHz. Part of the parameters for sharing study are summarized in Table 4, where the allowable interference power  $I_{th}$  is given by (4). For the worst case study, we adopted radars B and C with the lowest allowable interference powers among candidates, and assumed their peak antenna gains as the interference power at the radar receiver highly decreases in case of antenna sidelobe reception.

TABLE 3. Characteristics of IMT-Advanced base station in 3 GHz (over 3.3 GHz) frequency band.

Parameter	Units	Macro suburban	Macro urban	Micro urban
Carrier frequency	GHz	3.3	3.3	3.3
Signal bandwidth	MHz	10	10	10
Maximum output power	dBm/10 MHz	46	46	24
Antenna height	m	25	20	6
Maximum antenna gain	dBi	18	18	5
Downtilting	degrees	6	10	0
Antenna gain with downtilting	dBi	10.44	5.81	5
Feeder loss	dB	3	3	0
EIRP/10MHz	dBm	53.4	48.8	29
Below rooftop base station antenna deployment	%	0	50	100

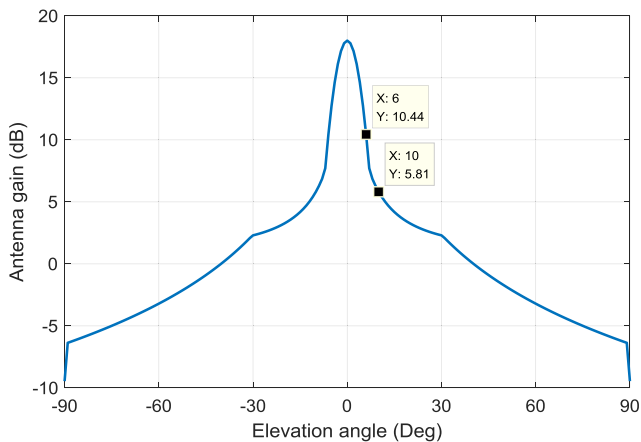


FIGURE 8. Elevation pattern of macro BS without downtilting at the zero azimuth angle.

Fig. 8 shows the antenna gain pattern in elevation of macro BS without downtilting for the zero azimuth angle. The gain pattern is computed by the reference radiation patterns of sectoral antennas for mobile services in the frequency range from 400 MHz to about 6 GHz given in section 3.1 of

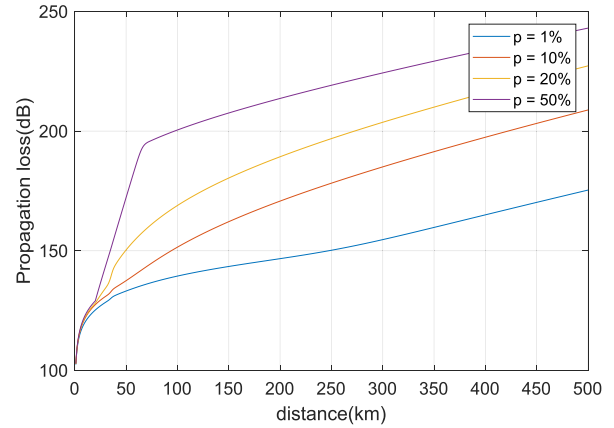


FIGURE 9. ITU-R Recommendation P.452 sea path loss for different time percentages.

Recommendation ITU-R F.1336 [52]. This recommendation is released to offer reference radiation patterns of omnidirectional, sectoral, and other antennas for the fixed and mobile services for use in sharing studies in the frequency range from 400 MHz to about 70 GHz. In Fig. 7, the antenna gain at zero elevation angle is 10.44 and 5.81 dBi for the downtilting of 6° and 10°, respectively. Considering antenna downtilting of 6° for suburban and 10° for urban in Table 2 and the assumption that the victim radar antenna is at zero elevation and azimuth angle, the antenna gains of 10.44 dB and 5.81 dB are adopted.

D. PROPAGATION MODEL AND INTERFERENCE CRITERIA

1) PROPAGATION MODEL

The propagation between IMT system and ship based radars is modeled by ITU-R recommendation P.452-16 [53]. Free software (Excel spreadsheet and MATLAB script) for the model implementation can be downloaded from ITU website [54]. The model is aimed at predicting interference potential between stations on the earth’s surface (land as well as sea) for frequencies in the range of approximately 0.1 GHz to 50 GHz. The model provides mathematical methods to compute propagation losses for time percentages over the range  $0.001\% \leq p \leq 50\%$ . The model outputs larger path loss for the higher time percentage as shown in Fig. 9, which informs stronger interference occurs for shorter periods of time. It should be noted that this assumption does not imply that the maximum loss will be at  $p = 50\%$ .

When  $p$  is a small percentage of the time, in the range  $0.001\% \leq p \leq 1\%$ , the interference is referred to as short term, whereas it is referred to as long term for  $p$  equal to or larger than 20% [55], [56]. The typical values of long term (20%) and short term (1%) interferences are evaluated in this study. The parameters of P.452 model adopted for this study are listed in Table 5, where the antenna height above the mean sea level equals the antenna height given in Table 2 and 3. Here, we assumed that the ground height above the mean sea level at transmitting or receiving station is zero.

2) CLUTTER MODEL

Recommendation ITU-R P.2108 [57] recently released three up-to-date models for computing clutter loss that refers to additional loss due to the wireless terminal antennas being embedded in local clutter (e.g., buildings, vegetation) in an urban or suburban environment at frequencies between 30 MHz and 100 GHz. Free software (Excel spreadsheet) for the model implementation is downloadable from the ITU website [54]. Two statistical models are provided to estimate clutter loss as a function of probability. One model (in section 3.2) addresses terrestrial paths, whereas the other model (in section 3.3) is for an inclined path where the terrestrial end of the path is within the clutter. Practical situations where clutter loss is negligible have also been accounted. These models have been developed using measurement results as well as analytical models, particularly in urban environments. The model in section 3.3 of the Recommendation is not applicable to BSs in the suburban open-space hotspot environment, because here the clutter loss is expected to be insignificant.

We adopted the clutter model that combines a percentage of above rooftop BSs without clutter loss and a percentage of below rooftop BSs with clutter loss defined in [57, Sec. 3.2], according to the percentages of below rooftop BS antenna deployment presented in Table 2. Clutter loss is therefore not applicable to the macro suburban BS with zero percentage of below rooftop antenna deployment. Fig. 10 plots a curve of clutter loss not exceeded for percentage  $q$ , of locations at 3.3 GHz, calculated by [57]

$$L_{clt} = -5 \log \left( 10^{-0.2L_l} + 10^{-0.2L_s} \right) - 6Q^{-1} (q/100), \quad (22)$$

where  $Q^{-1} (q/100)$  is the inverse complementary normal distribution function, and

$$L_l = 23.5 + 9.6 \log (f), \quad (23)$$

$$L_s = 32.98 + 23.9 \log (d) + 3 \log (f), \quad (24)$$

where  $f$  is the frequency in GHz and  $d$  is the total path length in km. Fig. 11 shows the median clutter loss computed by (22)

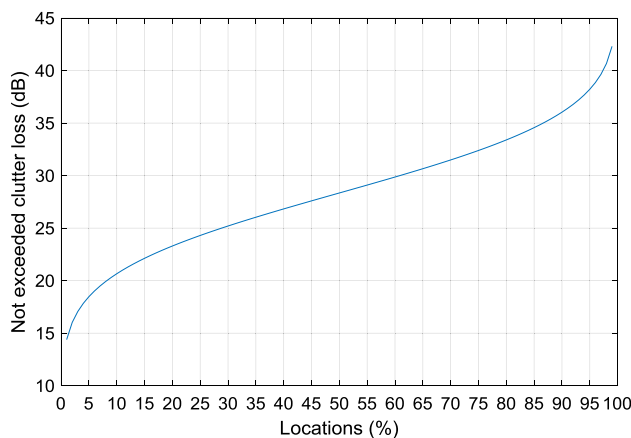


FIGURE 10. ITU-R Rec M.2108: Clutter loss not exceeded for percentage of locations for the distance larger than 1 km, at 3.3 GHz.

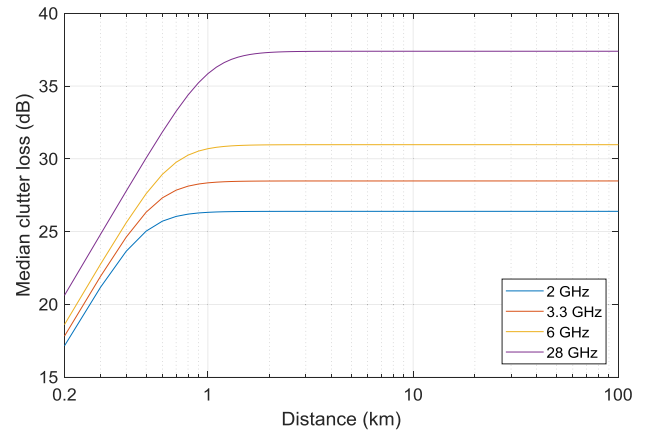


FIGURE 11. ITU-R Rec M.2108: median clutter loss for different frequencies.

TABLE 4. Characteristics of Radar in 3,100-3,700 MHz frequency band.

Parameter	Units	Ship-Based Radar B	Ship-Based Radar C
Antenna gain	dBi	42	40
Antenna height	m	20	20
Feeder loss	dB	0	0
Rx noise figure	dB	5.0	1.5
Rx IF bandwidth (-3 dB)	MHz	10	10
$INR_{th}$	dB	-6	-6
Allowable interference power $I_{th}$	dBm/10MHz z	-105	-108.5

TABLE 5. Parameters used propagation losses calculated with Rec. ITU-R Rec P.452.

Parameter	Unit	Value
Frequency	MHz	3,300
Latitude Transmitter	degrees	37.45
Longitude Transmitter	degrees	37.45
Latitude Receiver	degrees	126.59
Longitude Receiver	degrees	126.59
Transmitting ground height above mean sea level	m	0
Receiving ground height above mean sea level	m	0
Transmitting antenna height above mean sea level	m	25 (macro suburban), 20(macro urban), 6(micro urban)
Receiving antenna height above mean sea level	m	20
Sea-level surface refractivity	N-units	330
Average radio-refractive index lapse-rate	N-units/k m	45

with  $q = 50$  versus the total path length. The values increase for the path length but converge a certain value over about 1 km.

3) INTERFERENCE CRITERION

Signals received by radars from other systems could generate different types of degradation of performances. Desensitization is generally observed due to low level of interfering

**TABLE 6. Protection distance for radar B and C interfered with 5G BS with a linearized power amplifier.**

Radar	Guard band (MHz)	Percentage of time (%)	Protection distance (km)									
			Macro suburban			Macro urban			Micro urban			
			CP-OFDM	Windowed OFDM	Filtered OFDM	CP-OFDM	Windowed OFDM	Filtered OFDM	CP-OFDM	Windowed OFDM	Filtered OFDM	
B	0	1	383	3	0.003	37	0.057	< 0.001	2.8	0.006	< 0.001	
		20	86	2.5	0.003	25	0.057	< 0.001	2.6	0.006	< 0.001	
	1	1	361	0.273	< 0.001	29	0.007	< 0.001	2.1	< 0.001	< 0.001	
		20	78	0.264	< 0.001	20	0.007	< 0.001	2	< 0.001	< 0.001	
	5	1	321	0.020	< 0.001	17	< 0.001	< 0.001	1.3	< 0.001	< 0.001	
		20	68	0.020	< 0.001	13	< 0.001	< 0.001	1.3	< 0.001	< 0.001	
	10	1	291	0.006	< 0.001	11.6	< 0.001	< 0.001	0.864	< 0.001	< 0.001	
		20	61	0.006	< 0.001	8	< 0.001	< 0.001	0.835	< 0.001	< 0.001	
	20	1	253	0.002	< 0.001	7	< 0.001	< 0.001	0.585	< 0.001	< 0.001	
		20	54	0.002	< 0.001	5.9	< 0.001	< 0.001	0.57	< 0.001	< 0.001	
	C	0	1	397	3.2	0.004	43	0.068	< 0.001	3.4	0.007	< 0.001
			20	91	2.9	0.004	27	0.068	< 0.001	3	0.007	< 0.001
		1	1	376	0.324	< 0.001	34	0.008	< 0.001	2.5	< 0.001	< 0.001
			20	83	0.312	< 0.001	24	0.008	< 0.001	2.3	< 0.001	< 0.001
5		1	335	0.023	< 0.001	21	< 0.001	< 0.001	1.6	< 0.001	< 0.001	
		20	72	0.023	< 0.001	15	< 0.001	< 0.001	1.5	< 0.001	< 0.001	
10		1	307	0.006	< 0.001	14	< 0.001	< 0.001	1.1	< 0.001	< 0.001	
		20	65	0.006	< 0.001	11	< 0.001	< 0.001	0.987	< 0.001	< 0.001	
20		1	271	0.002	< 0.001	9	< 0.001	< 0.001	0.696	< 0.001	< 0.001	
		20	57	0.002	< 0.001	7	< 0.001	< 0.001	0.671	< 0.001	< 0.001	

**TABLE 7. Protection distance for radar B and C interfered with 5G BS with a nonlinear power amplifier ( $p = 2$ , IBO = -10 dB).**

Radar	Guard band (MHz)	Percentage of time (%)	Protection distance (km)									
			Macro suburban			Macro urban			Micro urban			
			CP-OFDM	Windowed OFDM	Filtered OFDM	CP-OFDM	Windowed OFDM	Filtered OFDM	CP-OFDM	Windowed OFDM	Filtered OFDM	
B	0	1	395	343	379	42	23	36	3.2	1.7	2.6	
		20	90	74	84	27	16	24	2.9	1.6	2.4	
	5	1	327	222	269	18	5.2	8.5	1.4	0.454	0.682	
		20	70	50	57	13	4.5	6.8	1.4	0.438	0.658	
	10	1	294	44	64	12	0.695	1.1	0.883	0.072	0.103	
		20	62	29	35	9	0.672	0.97	0.852	0.069	0.1	
	20	1	255	0.83	1.9	8	0.02	0.42	0.6	0.002	0.005	
		20	55	0.802	1.8	6	0.019	0.41	0.578	0.002	0.005	
	C	0	1	409	358	393	50	27	41	3.9	2.0	3.2
			20	94	78	89	29	19	27	3.5	1.9	2.9
5		1	341	243	286	22	6.4	11	1.7	0.540	0.807	
		20	73	53	60	16	5.3	8.1	1.6	0.521	0.780	
10		1	309	53	75	15	0.826	1.3	1.1	0.085	0.123	
		20	65	31	37	11	0.807	1.3	1.1	0.082	0.118	
20		1	273	0.987	2.3	8.9	0.024	0.050	0.713	0.003	0.006	
		20	58	0.953	2.1	7.1	0.023	0.048	0.687	0.003	0.006	

signals, and saturation or blocking of receivers could be observed for larger interfering signals. Recommendation ITU-R M.1465 [50] provides the radar interference criterion

in the radiolocation service given as  $INR_{th} = -6$  dB as shown in Table 4. An  $INR_{th}$  of  $-6$  dB results in a  $(I + N_R)/N_R$  of 1.26, i.e. about 1 dB increase in the radar receiver noise power.

**TABLE 8. Minimum FDR for fulfilling the  $INR_{th} = -6$  dB.**

BS type	Clutter loss (dB)	Percent age of time (%)	Minimum FDR (dB)			
			Radar B		Radar C	
			100m far from coastline	22 km far from coastline	100 m far from coastline	22 km far from coastline
Macro suburban	0	1	118	75	119	76
		20	118	72	119	73
Macro suburban	18	1	95	52	97	54
		20	95	49	97	51
	28	1	85	42	87	44
		20	85	39	87	41
Micro urban	18	1	76	32	77	34
		20	76	27	77	28
	28	1	66	22	67	24
		20	66	17	67	18

**V. COEXISTENCE BETWEEN 5G AND RADAR IN 3 GHz BAND: RESULTS FOR THE OFDM WAVEFORMS**

The A-MCL modeling developed in Sections II and III is applied to estimate the potential interference power from the 5G BS in a single entry worst case scenario as described in Section IV. The inference power is computed by (1), where the power, antenna gain, and feeder loss of a transmitter are given in Table 3, and the antenna gain and feeder loss of a receiver are given in Table 4. The propagation loss  $L_P$  is computed as the sum of the values of P.452 path loss and P.2018 clutter loss. No clutter loss is applied to the suburban macro BS, and median clutter loss of 28 dB is applied to the urban macro and micro BSs. Interference to noise power ratio is computed thereafter. The protection distance and the guard band are some of the basic technical parameters of spectrum management for ensuring a coexistence between 5G and other radio systems. We therefore analyze protection distance and guard band, and their tradeoffs for the coexistence. As the BS is assumed to be fixed at a shoreline, the protection distances refer to the minimum distance of the ship-based radar from the shoreline.

Tables 6 and 7 present protection distances for the ship-based radars interfered with the BS employing linearized amplifier and nonlinear amplifier, respectively. Since the FDR of CP-OFDM slowly decreases for increasing guard band as shown in Fig. 3, large protection distances (e.g. over 7 km for urban macro BS) are required for their coexistence even for a 20 MHz guard band. Much lower separation distances are required in the case of windowed OFDM (below 1 m for urban macro BS with a linearized amplifier in 1 MHz guard band and below 100 m for urban macro BS with a nonlinear amplifier in 20 MHz guard band) and filtered OFDM (below 1 m for urban macro BS in 0 MHz guard

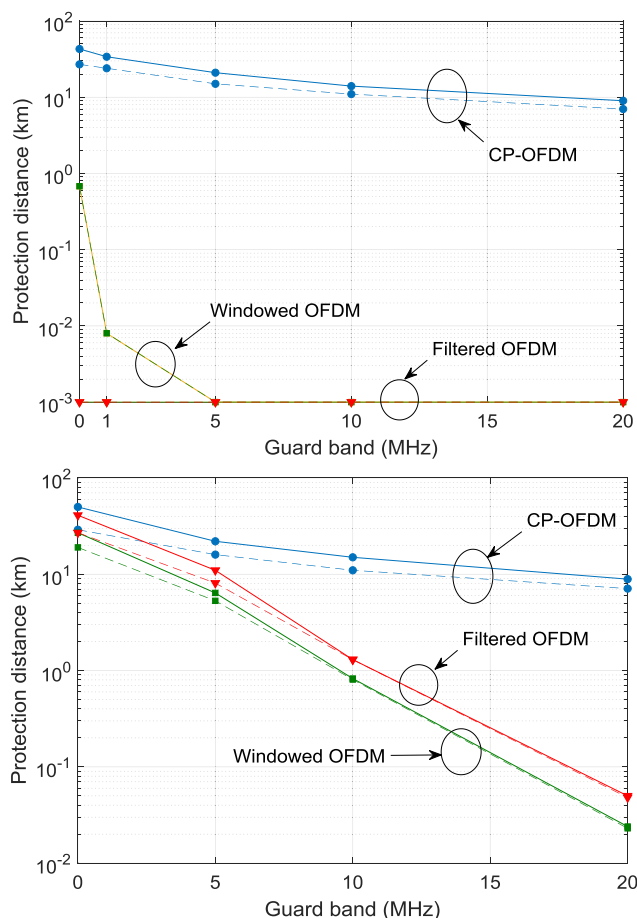


**FIGURE 12. Protection distance for radar C interfered with macro urban BS in the percentage time of 1% (solid line) and 20% (dashed line), for a linearized amplifier (upper figure) and a nonlinear amplifier (lower figure).**

band and below 100 m for urban macro BS with a nonlinear amplifier in 20 MHz guard band), due to their lower out-of-band emission.

These performance gaps are observed in Fig. 12. With a linearized amplifier, filtered OFDM and windowed OFDM respectively need approximately 0 MHz and 1 MHz guard bands for securing the 100 m protection distance, whereas CP-OFDM is incompetent even with the 20 MHz guard band. With a nonlinear amplifier, both filtered and windowed OFDM require much wider guard bands of approximately 18 MHz and 16 MHz for securing the 100 m protection distance, whereas CP-OFDM requires almost the same guard band as in the case of a linear amplifier. We also observed that the protection distances for 1 and 20 percentage are almost equal to or less than 1 km, because the propagation loss of sea path within several kilometers remains almost unchanged for varying time percentages, as shown in Fig. 9.

These numerical results indicate that with a linearized amplifier, filtered OFDM needs the shortest protection distance, whereas with a nonlinear amplifier, the windowed OFDM requires the shortest protection distance. As a result,

when considering nonlinearity of power amplifier, the performance gap between filtered and windowed OFDM is reduced, and the performance of both technologies can be reversed to the extent that the system variable changes. CP-OFDM needs the interference mitigation techniques listed in Table 1 to reduce its interference power at the radars. However, the spectrum manager or system designer should note that employing these techniques can involve performance loss of interfering systems.

Table 8 presents the minimum FDR for fulfilling the radar interference criterion for a given separation distance. The minimum FDR is computed by combining (3) and (4) as

$$FDR_{\min} = P_T - L_{FL,T} + G_T + G_R - L_{FL,R} - L_{POL} - L_P - INR_{th} - N_R. \quad (25)$$

These data can be useful for physical layer designers to directly map their current implementation to the coexistence condition.

## VI. CONCLUSION

The analytical expression of the FDR of CP-OFDM, windowed OFDM, and filtered OFDM are derived. To this end, the PSDs of CP-OFDM and windowed OFDM are reviewed, and the PSD of filtered OFDM with the Hanning window is newly derived. The FDR models are applied to the spectral coexistence study of 5G IMT systems with various types of radars. Both windowed and filtered OFDM require much shorter protection distance than CP-OFDM due to their lower out-of-band emissions. In the case of a linearized amplifier, the filtered OFDM IMT BS requires smaller protection distance compared to the windowed OFDM, whereas the windowed OFDM outperforms the filtered OFDM in the case of a nonlinear power amplifier. When considering nonlinear distortion of power amplifier, the sidelobe suppression performance of filtered and windowed OFDM can be highly dependent and can get reversed with changes in the system parameters such as the window length and filter order.

In addition to coexistence study, the proposed analytical expressions of the PSD and FDR can be applied to the system design of 5G or other new wireless systems with OFDM waveforms for i) investigating their compliance with regulatory spectrum masks, ii) allocating the guard subcarriers on either side of the OFDM channel band, iii) performance evaluation of the OFDM waveforms in a typical multiuser asynchronous access scheme, and iv) MC simulations to investigate the mutual inference of BS-to-BS, BS-to-UE, UE-to-UE conducted by the telecommunications standards such as the 3rd Generation Partnership Project (3GPP).

## APPENDIX

### A. FDR OF CP-OFDM

Assuming that subcarrier signals are statistically independent and mutually orthogonal, we derive the PSD of OFDM

signals by summing the PSD of each subcarrier as follows.

$$\begin{aligned} & \int_{\Delta f - W_v/2}^{\Delta f + W_v/2} \Phi_s(f) df \\ &= P_s T_{\text{tot}} \int_{\Delta f - W_v/2}^{\Delta f + W_v/2} \sum_{k=0}^{N-1} \left\{ \text{sinc} \left[ \left( f - \frac{k}{T_s} \right) T_{\text{tot}} \right] \right\}^2 df \\ &= P_s T_{\text{tot}} \int_{\Delta f - W_v/2}^{\Delta f + W_v/2} \sum_{k=0}^{N-1} \left\{ \frac{\sin \left[ \pi \left( f - \frac{k}{T_s} \right) T_{\text{tot}} \right]}{\pi \left( f - \frac{k}{T_s} \right) T_{\text{tot}}} \right\}^2 df. \end{aligned} \quad (26)$$

Let define symbols as  $t = \pi \left( f - k/T_s \right) T_{\text{tot}}$ ,  $f_u = \pi \left( \Delta f + W_v/2 \right) T_{\text{tot}}$ , and  $f_l = \pi \left( \Delta f - W_v/2 \right) T_{\text{tot}}$ , then (26) can be rewritten as

$$\int_{\Delta f - W_v/2}^{\Delta f + W_v/2} \Phi_s(f) df = P_s T_{\text{tot}} \sum_{k=0}^{N-1} \int_{f_l - kT_{\text{tot}}/T_s}^{f_u - kT_{\text{tot}}/T_s} \frac{\sin^2 t}{t^2} dt. \quad (27)$$

Using the equality of  $\int_a^b \sin^2(t)/t^2 dt = \sin^2(a)/a - \sin^2(b)/b - \text{Si}(2a) + \text{Si}(2b)$ , we obtain the FDR in (11).

### B. PSD OF WINDOWED OFDM

Since  $w_{rc}(t)$  is an even real function, its Fourier transform is simplified as

$$W_{rc}(f) = 2 \int_0^{\infty} w_{rc}(t) \cos(2\pi ft) dt. \quad (28)$$

Substituting (12) into (28) and using  $t_1 = (T_{\text{tot}} - T_{\text{tr}})/2$  and  $t_2 = (T_{\text{tot}} + T_{\text{tr}})/2$ , we obtain

$$\begin{aligned} W_{rc}(f) &= 2 \int_0^{t_1} \cos(2\pi ft) dt \\ &+ \int_{t_1}^{t_2} \left[ 1 + \cos \left( \frac{\pi(t - t_1)}{T_{\text{tr}}} \right) \right] \cos(2\pi ft) dt \\ &= \frac{\sin(2\pi ft_1) + \sin(2\pi ft_2)}{2\pi f} \\ &+ \frac{1}{2} \left[ \frac{\sin(2\pi ft_2) + \sin(2\pi ft_1)}{\pi(1/T_{\text{tr}} - 2f)} \right. \\ &\quad \left. - \frac{\sin(2\pi ft_2) + \sin(2\pi ft_1)}{\pi(1/T_{\text{tr}} + 2f)} \right] \\ &= [\sin(2\pi ft_1) + \sin(2\pi ft_2)] \\ &\quad \times \left[ \frac{1}{2\pi f} + \frac{2\pi f}{\left( \frac{\pi^2}{T_{\text{tr}}^2} - 4\pi^2 f^2 \right)} \right] \end{aligned} \quad (29)$$

Using  $\sin(x) + \sin(y) = 2 \sin((x+y)/2) \cos((x-y)/2)$ , the  $W_{rc}(f)$  can be expressed as

$$W_{rc}(f) = \frac{2 \sin(\pi f(t_1 + t_2)) \cos(\pi f(t_2 - t_1))}{2\pi f(1 - 4T_{\text{tr}}^2 f^2)}. \quad (30)$$

Substituting  $t_1 + t_2 = T_{\text{tot}}$  and  $t_2 - t_1 = T_{\text{tr}}$  into (27), we obtain

$$W_{rc}(f) = \frac{T_{\text{tot}} \text{sinc}(\pi f T_{\text{tot}}) \cos(\pi f T_{\text{tr}})}{(1 - 4T_{\text{tr}}^2 f^2)}. \quad (31)$$

Finally  $|P(f)|^2$  is expressed as

$$\begin{aligned} |P(f)|^2 &= \left| F \left\{ w_{rc} \left( t - \frac{T_{\text{tot}}}{2} \right) \right\} \right|^2 \\ &= \left| W_{rc}(f) e^{j\pi T_{\text{tot}} f} \right|^2 \\ &= \left[ \frac{T_{\text{tot}} \text{sinc}(\pi f T_{\text{tot}}) \cos(\pi f T_{\text{tr}})}{(1 - 4T_{\text{tr}}^2 f^2)} \right]^2. \end{aligned} \quad (32)$$

Substituting the above equation into (7), we obtain the PSD in (13).

### C. PSD OF FILTERED OFDM

The PSD of the filtered OFDM is given by

$$\begin{aligned} \Phi_x(f) &= |H(f)|^2 \Phi_s(f) \\ &= |G(f) * W(f)|^2 \Phi_s(f) \\ &= |G(f) * W(f)|^2 \Phi_s^{(\text{CP})}(f). \end{aligned} \quad (33)$$

The frequency response of the basic filter is given by

$$G(f) = \Pi \left( \frac{f}{W_g} \right), \quad (34)$$

The Fourier transform of the time-window function is given by

$$\begin{aligned} W(f) &= F \{ w(t) \} \\ &\stackrel{(a)}{=} 2 \int_0^{T_w/2} \frac{1}{2} \left( 1 + \cos \left( \frac{2\pi t}{T_w} \right) \right) \cos(2\pi f t) dt \\ &= \int_0^{T_w/2} \cos(2\pi f t) dt + \frac{1}{2} \int_0^{T_w/2} \cos \left( 2\pi \left( \frac{1}{T_w} + f \right) t \right) dt \\ &\quad + \frac{1}{2} \int_0^{T_w/2} \cos \left( 2\pi \left( \frac{1}{T_w} - f \right) t \right) dt \\ &= \frac{\sin(\pi T_w f)}{2\pi f} - \frac{\sin(\pi T_w f)}{4\pi (1/T_w + f)} + \frac{\sin(\pi T_w f)}{4\pi (1/T_w - f)} \\ &= \sin(\pi T_w f) \left[ \frac{1}{2\pi f (1 - T_w^2 f^2)} \right] \\ &= \frac{T_w \text{sinc}(T_w f)}{2(1 - T_w^2 f^2)}, \end{aligned} \quad (35)$$

where (a) is given because  $w(t)$  is an even real function. The convolution of  $G(f)$  and  $W(f)$  is given by

$$\begin{aligned} G(f) * W(f) &= \int_{-\infty}^{\infty} G(\phi) W(f - \phi) d\phi \\ &= \frac{T_w}{2} \int_{-\infty}^{\infty} \Pi \left( \frac{\phi}{W_g} \right) \frac{\text{sinc}(T_w(f - \phi))}{(1 - T_w^2(f - \phi)^2)} d\phi \\ &= \frac{T_w}{2} \int_{-W_g/2}^{W_g/2} \frac{\text{sinc}(T_w(f - \phi))}{(1 - T_w^2(f - \phi)^2)} d\phi, \end{aligned} \quad (36)$$

Using the substitutions  $t = T_w(f - \phi)$ ,  $f_u = T_w(f + W_g/2)$ , and  $f_l = T_w(f - W_g/2)$ , the convolution is rewritten as,

$$\begin{aligned} G(f) * W(f) &= \frac{1}{2} \int_{f_l}^{f_u} \frac{\text{sinc}(t)}{1 - t^2} dt \\ &\stackrel{(a)}{=} \frac{1}{4\pi} [2\text{Si}(\pi f_u) - 2\text{Si}(\pi f_l) + \text{Si}(\pi - \pi f_l) \\ &\quad - \text{Si}(\pi - \pi f_u) + \text{Si}(\pi + \pi f_u) - \text{Si}(\pi + \pi f_l)] \end{aligned} \quad (37)$$

where (a) is given from  $\int \text{sinc}(t)/(1 - t^2) dt = [2\text{Si}(\pi t) - \text{Si}(\pi - \pi t) + \text{Si}(\pi + \pi t)] / (2\pi)$ . Substituting (37) into (33), we obtain the PSD expression in (18).

### REFERENCES

- [1] X. Zhang, M. Jia, L. Chen, J. Ma, and J. Qiu, "Filtered-OFDM—Enabler for flexible waveform in the 5th generation cellular networks," in *Proc. IEEE Global Commun. Conf. (GLOBECOM)*, San Diego, CA, USA, Dec. 2015, pp. 1–6.
- [2] H. Tullberg, "The METIS 5G system concept: Meeting the 5G requirements," *IEEE Commun. Mag.*, vol. 54, no. 12, pp. 132–139, Dec. 2016.
- [3] A. D. S. Jayalath and C. Tellambura, "Reducing the out-of-band radiation of OFDM using an extended guard interval," in *Proc. IEEE 54th Veh. Technol. Conf. (VTC Fall)*, Atlantic City, NJ, USA, vol. 2, Oct. 2001, pp. 829–833.
- [4] C. Liu and F. Li, "Spectrum modelling of OFDM signals for WLAN," *Electron. Lett.*, vol. 40, no. 22, pp. 1431–1432, Oct. 2004.
- [5] M. Bellanger et al., "FBMC physical layer: A primer," *PHYDYAS*, vol. 25, no. 4, pp. 7–10, Jan. 2010.
- [6] B. Farhang-Boroujeny, "OFDM versus filter bank multicarrier," *IEEE Signal Process. Mag.*, vol. 28, no. 3, pp. 92–112, May 2011.
- [7] A. Sahin, I. Guvenc, and H. Arslan, "A survey on multicarrier communications: Prototype filters, lattice structures, and implementation aspects," *IEEE Commun. Surveys Tuts.*, vol. 16, no. 3, pp. 1312–1338, 3rd Quart., 2012.
- [8] V. Vakilian, T. Wild, F. Schaich, S. T. Brink, and J.-F. Frigon, "Universal-filtered multi-carrier technique for wireless systems beyond LTE," in *Proc. IEEE Globecom Workshops (GC Wkshps)*, Dec. 2013, pp. 223–228.
- [9] J. Abdoli, M. Jia, and J. Ma, "Filtered OFDM: A new waveform for future wireless systems," in *Proc. IEEE 16th Int. Workshop Signal Process. Adv. Wireless Commun. (SPAWC)*, Stockholm, Sweden, Jun./Jul. 2015, pp. 66–70.
- [10] Y. Li, X. Sha, and L. Ye, "Downlink resource sharing for D2D communications in a filtered OFDM system," in *Proc. IEEE 83rd Veh. Technol. Conf. (VTC Spring)*, Nanjing, China, May 2016, pp. 1–6.
- [11] Y. Qiu, Z. Liu, and D. Qu, "Filtered bank based implementation for filtered OFDM," in *Proc. 7th IEEE Int. Conf. Electron. Inf. Emergency Commun. (ICEIEC)*, Macau, China, Jul. 2017, pp. 15–18.
- [12] L. Zhang, A. Ijaz, P. Xiao, M. M. Molu, and R. Tafazolli, "Filtered OFDM systems, algorithms, and performance analysis for 5G and beyond," *IEEE Trans. Commun.*, vol. 66, no. 3, pp. 1205–1218, Mar. 2018.
- [13] J. Yli-Kaakinen et al., "Efficient fast-convolution-based waveform processing for 5G physical layer," *IEEE J. Sel. Areas Commun.*, vol. 35, no. 6, pp. 1309–1326, Jun. 2017. doi: 10.1109/JSAC.2017.2687358.
- [14] T. Levanen, J. Pirskanen, K. Pajukoski, M. Renfors, and M. Valkama, "Transparent Tx and Rx waveform processing for 5G new radio mobile communications," *IEEE Wireless Commun.*, vol. 26, no. 1, pp. 128–136, Feb. 2019. doi: 10.1109/MWC.2018.1800015.
- [15] Qualcomm. (2017). *Spectrum for 4G and 5G*. [Online]. Available: <https://www.qualcomm.com/media/documents/files/spectrum-for-4g-and-5g.pdf>
- [16] GSMA. (2016). *5G Spectrum Public Policy Position*. [Online]. Available: <https://www.gsma.com/spectrum/wp-content/uploads/2016/06/GSMA-5G-Spectrum-PPP.pdf>
- [17] *Resolution 223 (REV.WRC-15): Additional Frequency Bands Identified for International Mobile Telecommunications*, document Final Acts WRC-15, World Radiocommunication Conference, ITU, Geneva, Switzerland, 2015.
- [18] *Sharing Studies Between IMT-Advanced and the Radiolocation Service in the 3,400–3,700 MHz Bands*, document ITU-R Rep. M.2111, Mar. 2008.

- [19] H.-S. Jo, H.-G. Yoon, J. Lim, W.-G. Chung, J.-G. Yook, and H.-K. Park, "The coexistence of OFDM-based systems beyond 3G with fixed service microwave systems," *J. Commun. Netw.*, vol. 8, no. 2, pp. 187–193, Jun. 2006.
- [20] W.-G. Chung, H.-S. Jo, H.-G. Yoon, J.-W. Lim, J.-G. Yook, and H.-K. Park, "Advanced MCL method for sharing analysis of IMT-advanced systems," *Electron. Lett.*, vol. 42, no. 21, pp. 1234–1235, Oct. 2006.
- [21] Z. A. Shamsan, "Bandwidth overlap factor for feasible coexistence of LTE-A and point to multipoint LMDS systems," *Wireless Pers. Commun.*, vol. 97, no. 2, pp. 2017–2035, Nov. 2017.
- [22] Z. A. Shamsan and A. M. Al-Hetar, "An improved mathematical scheme for LTE-advanced coexistence with FM broadcasting service," *PLoS ONE*, vol. 11, no. 11, Nov. 2016, Art. no. e0136912.
- [23] Z. A. Shamsan, T. A. Rahman, M. R. Kamarudin, A. M. Al-Hetar, and H.-S. Joss, "Coexistence of OFDM-based IMT-advanced and FM broadcasting systems," *ETRI J.*, vol. 33, no. 2, pp. 279–282, Apr. 2011.
- [24] S.-S. Raymond, A. Abubakari, H.-S. Jo, H.-J. Hong, and H. K. Son, "Compatibility between LTE and airport surveillance radar in 2700–2900 MHz radar bands," in *Proc. Int. Conf. Inf. Commun. Technol. Converg. (ICTC)*, Oct. 2015, pp. 1037–1042.
- [25] S.-S. Raymond, A. Abubakari, and H.-S. Jo, "Coexistence of power-controlled cellular networks with rotating radar," *IEEE J. Sel. Areas Commun.*, vol. 34, no. 10, pp. 2605–2616, Oct. 2016.
- [26] A. Khawar, A. Abdel-Hadi, and T. C. Clancy, "Spectrum sharing between S-band radar and LTE cellular system: A spatial approach," in *Proc. IEEE Int. Symp. Dyn. Spectr. Access Netw.*, Apr. 2014, pp. 7–14.
- [27] Y. Noam and A. J. Goldsmith, "Blind null-space learning for MIMO underlay cognitive radio with primary user interference adaptation," *IEEE Trans. Wireless Commun.*, vol. 12, no. 4, pp. 1722–1734, Apr. 2013.
- [28] F. Guidolin, M. Nekovee, L. Badia, and M. Zorzi, "A study on the coexistence of fixed satellite service and cellular networks in a mmWave scenario," in *Proc. IEEE Int. Conf. Commun. (ICC)*, London, U.K., Jun. 2015, pp. 2444–2449.
- [29] F. Guidolin and M. Nekovee, "Investigating spectrum sharing between 5G millimeter wave networks and fixed satellite systems," in *Proc. IEEE Globecom Workshops (GC Wkshps)*, San Diego, CA, USA, Dec. 2015, pp. 1–7.
- [30] S. Kim, E. Visotsky, P. Moorut, K. Bechta, A. Ghosh, and C. Dietrich, "Coexistence of 5G with the incumbents in the 28 and 70 GHz bands," *IEEE J. Sel. Areas Commun.*, vol. 35, no. 6, pp. 1254–1268, Jun. 2017.
- [31] G. Hattab, E. Visotsky, M. Cudak, and A. Ghosh, "Coexistence of 5G mmWave users with incumbent fixed stations over 70 and 80 GHz," in *Proc. IEEE Globecom Workshops (GC Wkshps)*, Singapore, Dec. 2017, pp. 1–5.
- [32] W. A. Hassan, H.-S. Jo, and A. R. Tharek, "The feasibility of coexistence between 5G and existing services in the IMT-2020 candidate bands in Malaysia," *IEEE Access*, vol. 5, pp. 14867–14888, 2017.
- [33] J. Kim, L. Xian, and A. S. Sadri, "Numerical simulation study for frequency sharing between millimeter-wave systems and fixed service systems in millimeter-wave bands," *IEEE Access*, vol. 4, pp. 9847–9859, 2016.
- [34] T. Levanen et al., "5G new radio and LTE uplink coexistence," in *Proc. IEEE Wireless Commun. Netw. Conf. (WCNC)*, Barcelona, Spain, Apr. 2018, pp. 1–6. doi: 10.1109/WCNC.2018.8377165.
- [35] *A Comparison of the Minimum Coupling Loss Method, Enhanced Minimum Coupling Loss Method, and the Monte-Carlo Simulation*, document CEPT ERC Rep. 101, May 1999.
- [36] *Modelling and Simulation of IMT Networks and Systems for use in Sharing and Compatibility Studies*, document ITU-R Rec. M.2101-0, Feb. 2017.
- [37] *Procedures for Determining the Potential for Interference Between Radars Operating in the Radiodetermination Service and Systems in Other Services*, document ITU-R Rec. M.1461-2, Jan. 2018.
- [38] *Frequency and Distance Separations*, document ITU-R Rec. SM.337-6, Oct. 2008.
- [39] S. H. Raghavan and H. Chew, "Frequency-dependent rejection, spectral separation coefficient, and interference analysis," in *Proc. IEEE Aerosp. Conf.*, Big Sky, MT, USA, Mar. 2018, pp. 1–10.
- [40] S. Hu, G. Wu, J.-J. Ping, and S.-Q. Li, "HPA nonlinearity reduction by joint predistorter and tone-reservation with null subcarriers in WiMAX systems," in *Proc. 4th IEEE Int. Conf. Circuits Syst. Commun.*, Shanghai, China, May 2008, pp. 187–190.
- [41] S. Hu, G. Wu, Q. Wen, Y. Xiao, and S. Li, "Nonlinearity reduction by tone reservation with null subcarriers for WiMAX system," *Wireless Pers. Commun.*, vol. 54, no. 2, pp. 289–305, 2010.
- [42] R. N. Braithwaite, "Implementing crest factor reduction (CFR) by offsetting digital predistortion (DPD) coefficients," in *Proc. Workshop Integr. Nonlinear Microw. Millimetre-Wave Circuits*, Dublin, Ireland, Sep. 2012, pp. 1–3.
- [43] C. Rapp, "Effects of HPA-nonlinearity on a 4-DPSK/OFDM-signal for a digital sound broadcasting signal," in *Proc. 2nd Eur. Conf. Satell. Commun.*, Oct. 1991, pp. 179–184.
- [44] S. C. Cripps, *RF Power Amplifiers for Wireless Communications*, 2nd ed. Norwood, MA, USA: Artech House, 2006.
- [45] M. Webster, "Suggested PA model for 802.11 HRb," Tech. Rep., Sep. 2000.
- [46] E. Perahia, "IEEE P802.11 wireless LANs TGad evaluation methodology," Tech. Rep., Sep. 2010.
- [47] C. Dehos and T. C. W. Schenck, "Digital compensation of amplifier nonlinearities in the receiver of a wireless system," in *Proc. 14th IEEE Symp. Commun. Veh. Technol. Benelux*, Nov. 2007, pp. 1–6.
- [48] *Frequency Allocations*, ITU Radio Regulations, Geneva, Switzerland, vol. 1, 2016.
- [49] *Preliminary Draft New Report ITU-R.M.[RADAR3300]—Sharing Between Indoor IMT Systems and Radar Systems in the Frequency Band 3 300-3 400 MHz*, document Annex 32-Report on the sixth and final meeting of Joint Task Group 4-5-6-7, Jul. 2014.
- [50] *Characteristics of and Protection Criteria for Radars Operating in the Radiodetermination Service in the Frequency Band 3,100–3,700 MHz*, document ITU-R Rec. M.1465-3, Jan. 2018.
- [51] *Characteristics of Terrestrial IMT-Advanced Systems for Frequency Sharing/ Interference Analyses*, document ITU-R Rec. M.2292-0, Dec. 2013.
- [52] *Reference Radiation Patterns of Omnidirectional, Sectoral and Other Antennas for the Fixed and Mobile Services for use in Sharing Studies in the Frequency Range from 400 MHz to About 70 GHz*, document ITU-R Rec. F.1336-4, Feb. 2014.
- [53] *Prediction Procedure for the Evaluation of Interference Between Stations on the Surface of the Earth at Frequencies Above About 0.1 GHz*, document Rec. ITU-R P.452-16, 2015.
- [54] *Software, Data and Validation Examples for Ionospheric and Tropospheric Radio Wave Propagation and Radio Noise*. [Online]. Available: <https://www.itu.int/en/ITU-R/study-groups/rsg3/Pages/iono-tropospheric.aspx>
- [55] *Determination of the Interference Potential Between Earth Stations of the Fixed-Satellite Service and Stations in the Fixed Service*, document ITU-R Rec. SF.1006, Apr. 1993.
- [56] *Considerations in the Development of Criteria for Sharing Between the Terrestrial Fixed Service and Other Services*, document ITU-R Rec. F.758-4, Jan. 2005.
- [57] *Prediction of Clutter Loss*, document ITU-R Rec. P.2108-0, Jun. 2017.



**JAEDON PARK** received the B.S. degree in electronics engineering from Hanyang University, Seoul, South Korea, in 2000, and the M.S. and Ph.D. degrees from the School of Electrical Engineering, Korea Advanced Institute of Science and Technology (KAIST), Daejeon, South Korea, in 2002 and 2016, respectively.

He is currently a Senior Researcher with the Agency for Defense Development (ADD), Daejeon. His research interests include MIMO systems, relay systems, and FSO systems.



**EUNHYOUNG LEE** received the B.S. degree in electronics engineering from Sungkyunkwan University, Seoul, South Korea, in 1983, and the M.S. degree in electronics engineering from Cheongju University, South Korea, in 1994.

He is currently a Principal Researcher with the Agency for Defense Development (ADD), Daejeon, South Korea. His research interests include electro-magnetic spectrum operations (EMSOs) and cyber electro-magnetic activity (CEMA).



**SUNG-HO PARK** (M'87) received the B.S. degree in mathematics from Korea University, Seoul, South Korea, in 1984.

From 1985 to 2005, he was working in software company for word-processor, middle-ware, and software for financial industry. Since 2005, he has been developing spectrum management and analysis software for government and military. He is currently developing spectrum analysis software for military operation.



**SEONGMIN PYO** (S'09–M'11–SM'15) received the B.E., M.E., and Ph.D. degrees in radio communication and engineering from Korea University, Seoul, South Korea, in 2002, 2004, and 2011, respectively.

In 2011, he was a Senior Researcher with the Electronics and Telecommunications Research Institute (ETRI). He developed a metamaterial-based microwave/millimeter-wave and THz imaging/spectroscopy systems. In 2011, he joined the Agency for Defense Development (ADD), where he was a Senior Researcher and involved communication waveform scanning and monopulse tracking systems for unmanned aerial vehicles. In 2013, he joined Hanbat National University, Daejeon, South Korea, where he is currently an Associate Professor with the Department of Information and Communication Engineering. He is also with The University of Texas at Arlington, Arlington, TX, USA, as a Visiting Scholar. His research interests include electromagnetic theories, reconfigurable antennas, RF and microwave components, and wave propagations.

Dr. Pyo has been a Committee Member of the IEEE Daejeon Section, since 2014, and the Institute of Civil Military Technology Cooperation (ICMTC), since 2017. He was a recipient of the South Korea Research Foundation BrainKorea21 Graduate Fellowship, from 2008 to 2010, and the Outstanding Graduate Ph.D. Fellowship presented by the Graduate School, Korea University, from 2009 to 2010. He appears in Marquis' Who's Who in the World, from 2011 to 2018.



**SABOGU-SUMAH RAYMOND** (S'16) was born in Ghana. He received the B.Sc. degree (Hons.) in telecommunications engineering from the Kwame Nkrumah University of Science and Technology, Kumasi, Ghana, in 2013, and the master's degree from Hanbat National University, Daejeon, South Korea.

He was a Researcher with the Artificial Intelligence for Networks Laboratory, University of Oklahoma, USA. He is currently an Engineer with the National Communications Authority, Ghana, and an Associate with the Wireless Communications and Networks Laboratory, Hanbat National University. His research interests include spectrum sharing, coexistence between wireless services, millimeter-wave communications, and 5G technology.



**HAN-SHIN JO** (S'06–M'10) received the B.S., M.S., and Ph.D. degrees in electrical and electronics engineering from Yonsei University, Seoul, South Korea, in 2001, 2004, and 2009, respectively.

He was a Postdoctoral Research Fellow with the Wireless Network and Communications Group, Department of Electrical and Computer Engineering, The University of Texas at Austin, from 2009 to 2011. He developed a long-term evolution base station at Samsung Electronics, from 2011 to 2012. He is currently an Associate Professor with the Department of Electronics and Control Engineering, Hanbat National University, Daejeon, South Korea. His current research interests include all the aspects of MIMO (channel modeling, precoding and scheduling with limited feedback, beamforming, SDMA, and massive MIMO) and applications of stochastic geometry, and optimization theory to wireless cellular and ad hoc networks. He was a recipient of the Samsung Electronics Graduate Fellowship, from 2006 to 2008, the Korea Research Foundation BrainKorea21 Graduate Fellowship, from 2006 to 2007, the Korea Research Foundation Postdoctoral Fellowship, in 2009, and the 2011 ETRI Journal Best Paper Award.

...